RSC Advances

PAPER

View Article Online
View Journal | View Issue

Cite this: *RSC Adv.*, 2017, **7**, 50949

One-pot synthesis of water-soluble near-infrared fluorescence RNase A capped $CuInS_2$ quantum dots for *in vivo* imaging

Yue Xi,†[a] Jianjun Yang,†[a] Yunshen Ge,[b] Shenli Zhao,[a] Jianguang Wang,[a] Yunxia Li,[b] Yuefeng Hao,*[c] Jun Chen *[b] and Yuchang Zhu*[a]

Received 31st July 2017
Accepted 10th October 2017

DOI: 10.1039/c7ra08418h

rsc.li/rsc-advances

Near-infrared (NIR) quantum dots (QDs) have been treated as a promising candidate of imaging agents for NIR fluorescence-guided surgery. Herein, one-pot synthesis of water-soluble NIR fluorescence $CuInS_2$ QDs was developed using ribonuclease A (RNase A) as the template. Our product exhibits good colloidal stability, excellent NIR fluorescence properties, and good photostability, even under acidic conditions. Furthermore, the RNase A-$CuInS_2$ QDs have minor suppression on cell viability even at a concentration of up to 5 mg mL^{-1}. Finally, the following *in vivo* imaging results confirm that RNase A-$CuInS_2$ QDs can be used as a novel oral imaging agent in the future.

Introduction

In recent years, near-infrared (NIR), especially in the range of 700–900 nm, -guided surgery as an emerging state-of-the-art technology is becoming significantly popular in the clinic because it can provide more anatomic and functional information from visible to NIR regions.[1,2] To date, this technique has been successfully applied for the visualization of sentinel lymph node in cancer resection surgery, evaluation of blood circulation for flap perfusion, and intraoperative location of brain vascular malformations.[3–7] Normally, an NIR-guided surgery system mainly consists of an organic dye and an NIR imaging device. To the best of our knowledge, only indocyanine green (ICG) as the NIR contrast agent has been approved by the FDA and European medicines agency (EMA). ICG is a water-soluble anionic, amphiphilic fluorophore with an emission around 830 nm and is being used in the clinic since 1957.[8–10] However, like other organic dyes, ICG has some drawbacks such as unstable fluorescence signals in either biological environment or during continuous laser excitation. Thus, a more stable NIR imaging agent is still strongly needed for the development of NIR-guided surgery now.

Compared to the traditional organic dyes, quantum dots (QDs) show many unique advantages such as size-tunable fluorescence, high quantum yields, and good photostability.[11,12] Recently, various kinds of studies on the synthesis of NIR QDs, such as HgTe, CdHgTe, CdTeSe, CdTeSe/CdS, PbS, and Au/PbS QDs, have been reported.[13–18] However, the toxicity of Cd and Hg has prompted the search for non-toxic materials. Particularly, $CuInS_2$ QDs with a narrow band gap (1.45 eV) are treated as promising candidates for the NIR imaging agent.[19] In this study, to further improve the water-solubility and biocompatibility, one-pot synthesis route of the NIR-emitting $CuInS_2$ QDs has been successfully demonstrated using ribonuclease A (RNase A) as a stabilizer in the water phase. RNase A is selected because of its excellent stability at high temperatures.[20] The morphology and optical properties of the as-prepared QDs were characterized using X-ray diffraction (XRD), high-resolution transmission electron microscopy (HR-TEM), UV-vis absorption spectroscopy, and photoluminescence (PL) techniques. Moreover, the cytotoxicity and *in vitro* stability of the as-prepared QDs were assessed. In addition, both *in vivo* imaging and gastrointestinal tract imaging were employed to demonstrate their advantages in biomedical imaging.

Materials and methods

Material reagents

Copper(I) iodide (CuI, 99.99%), indium acetate ($InAc_3$, 99.99%), ribonuclease A, sodium hydroxide (NaOH), and sulfourea ($CS(NH_2)_2$) were purchased from Sigma-Aldrich Corporation. Water used in all experiments had a resistivity higher than 18 MΩ cm^{-1}. Dulbecco's modified Eagle's medium (DMEM) with high glucose was obtained from Invitrogen Corporation. Phosphate buffer saline (PBS) was supplied by Shanghai Sangon, Ltd.

Synthesis of RNase A-$CuInS_2$ QDs

The RNase A-$CuInS_2$ nanoparticles were synthesized according to our previously reported method with some modifications.[11,21–25] In

[a]Department of Orthopaedics, Tenth People's Hospital of Tongji University, Shanghai, 2000072, China. E-mail: drzhuyuchang@163.com
[b]Department of Orthopedic Sports Medicine, Huashan Hospital, Fudan University, Shanghai 200040, China. E-mail: biochenjun@fudan.edu.cn
[c]Sports Medicine Center, Affiliated Suzhou Hospital of Nanjing Medical University, Suzhou Municipal Hospital, Suzhou, 21500, China. E-mail: 13913109339@163.com
† These authors are contributed equally.

a typical core synthesis, at first, the initial precursors CuI (0.2 mM), $InAc_3$ (0.2 mM), and RNase A (50 mg mL^{-1}) were mixed. Then, 200 μL of 1 M NaOH was added to this mixture. Afterward, the reaction temperature was increased to 100 °C, solution was kept at this temperature for 1 min, and the RNase A $CuInS_2$ QDs were obtained.

Characterization

TEM analysis was performed using an FEI Tecnai F20 field emission gun TEM/STEM microscope operated at 200 kV. X-ray diffraction patterns were obtained using a Bruker Advance powder X-ray diffractometer *via* a Cu Kα radiation ($\lambda = 1.5406$ Å). UV-vis-NIR spectra were obtained using a LAMBDA 950 UV/vis/NIR spectrophotometer. The photoluminescence (PL) stability of the QDs was examined using an Edinburgh FS 900 CDT fluorometer (Edinburgh Analytical Instruments).

In vitro evaluation of the as-prepared QDs

Mouse calvaria-derived cell lines (MC3T3-E1) were purchased from the Cell Bank of the Chinese Academy of Sciences Type Culture Collection and cultured in DMEM supplemented with 10% FBS (Sigma Chemical, St. Louis, MO), 100 units mL^{-1} penicillin, and 0.1 mg mL^{-1} streptomycin. The cells were stored at 37 °C in a humidified chamber with 5% CO_2, and then, the culture was expanded with moderate changes every three days.

The cytotoxicity of the RNase A-$CuInS_2$ QDs to MC3T3-E1 cells was determined using an MTT cytotoxicity assay. The cells were cultured with 0, 0.05, 0.5, and 5 mg mL^{-1} of the RNase A-$CuInS_2$ QDs for 24 h. Then, cell viabilities were measured using a standard MTT assay kit according to the manufacturer's instructions.

The stability of the RNase A-$CuInS_2$ QDs was evaluated by storing them at different temperatures (4 °C, 37 °C, and 60 °C) and in different buffers (PBS, distilled water, and DMEM) for 96 h. The fluorescence intensity of the QDs was detected at different time intervals (0, 24 h, 48 h, and 96 h) using the Edinburgh FS 900 CDT fluorometer.

In vivo imaging

Herein, four- to six-week-old nude female mice were obtained from the Experimental Animal Center of the Chinese Academy of Sciences in Shanghai, China. The study was performed within the Guidelines for the Care and Use of Research Animals. The study was approved by the Animal Care and Use Committee and the Ethics Committee of Shanghai Tenth People's Hospital and Tenth People's Hospital of Tongji University. The mice received a single intravenous injection of 200 μL RNase A-$CuInS_2$ QDs by either a normal or a gastric syringe. The *in vivo* images were obtained using an optical and X-ray small animal imaging system (*In vivo* Xtreme, American Bruker). These *in vivo* images were further utilized for the surface plot analysis using the ImageJ software (National Institutes of Health, USA). The mice were satisfied after 10 min treatment of the QDs, and six organs were obtained for *ex vivo* analysis.

Result and discussion

Characterization

As shown in Fig. 1A, the TEM image of the as-prepared RNase A-$CuInS_2$ QDs showed that our product was monodispersed in the water solution, and the QDs had the unique morphology of spherical particles. Furthermore, the HR-TEM image (as shown in Fig. 1) of a single RNase A-$CuInS_2$ QD clearly demonstrated its good crystal structure with clear lattice fringes. Notably, the RNase A protein was not observed due to the low contrast of biomolecules in the TEM image; the size of the RNase A-$CuInS_2$ QDs in the TEM image was calculated to be 3.25 nm, which was in accordance with that obtained from the HR-TEM images.

In addition, XRD was carried out to confirm the successful synthesis of the RNase A-$CuInS_2$ QDs. As shown in Fig. 2, three main diffraction peaks in the XRD pattern of our product appeared at around 28°, 47°, and 55°, which present a typical zinc blende (cubic) structure without impurities (JCDPS #85-1575), in agreement with those reported in the previous study.[9]

In this study, the chemicals with a fixed precursor ratio of Cu : In : S (1 : 1 : 2) were introduced into distilled water, and the Cu^{2+} precursor concentration was further investigated. Fig. 3A shows the relationship between the Cu^{2+} concentration and the PL intensity of the RNase A-$CuInS_2$ QDs. The fluorescence peak of the RNase A-$CuInS_2$ QDs was around 780 nm when the Cu^{2+} concentration was 0.5 mM. Appealingly, the PL intensity of the QDs gradually increased correspondingly with the increase in the Cu^{2+} concentration from 0.5 mM to 10 mM, whereas the position of the fluorescence emission peak showed no obvious shift. It shows that the RNase A-$CuInS_2$ QDs can be synthesized at a low precursor concentration in our study, and the bulk cannot be produced by increasing the concentration. Moreover, the reaction temperature is considered as a key factor for the synthesis of the water-soluble QDs according to our previous studies.[18–22] Thus, different temperatures were also investigated in this study. As shown in Fig. 3B, the fluorescence emission spectra of a given sample at different reaction temperatures revealed that the emission peak of the QDs systematically shifted from 760 nm to 830 nm due to the quantum size effect. Furthermore, our products showed a single well-defined exciton peak, which suggested that there was no structural inhomogeneity.

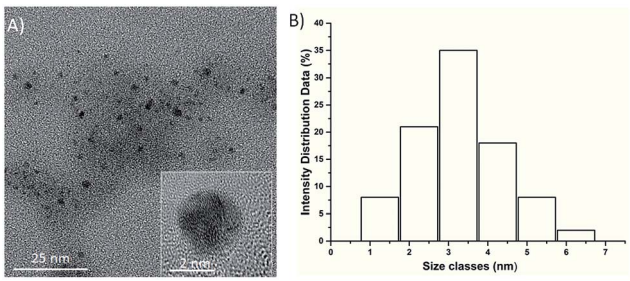

Fig. 1 (A) TEM image of RNase A-$CuInS_2$ QDs. The inset: an HR-TEM image of a single RNase A-$CuInS_2$ QD and (B) the size distribution analysis of the RNase A-$CuInS_2$ QDs.

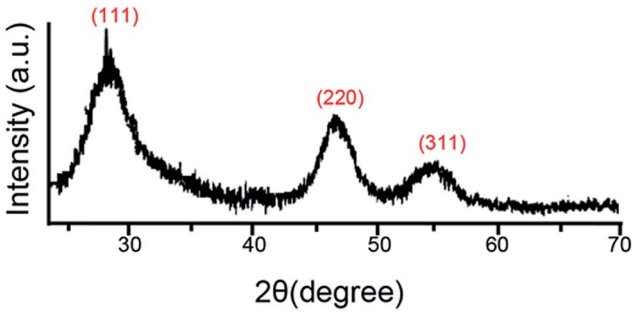

Fig. 2 The X-ray diffraction (XRD) pattern of the as-prepared RNase A-$CuInS_2$ QDs.

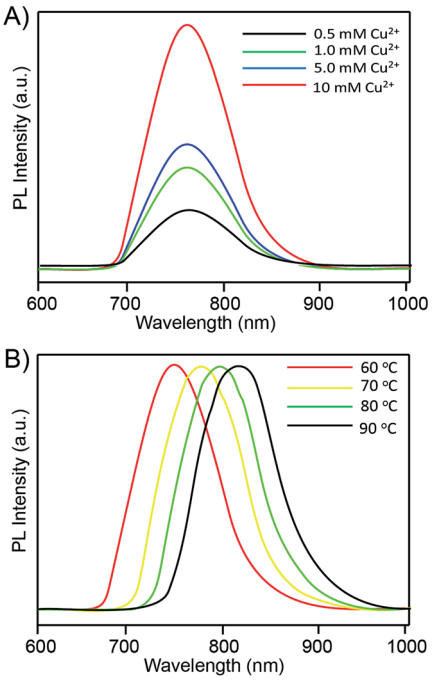

Fig. 3 (A) The fluorescence emission spectra of the as-prepared RNase A-$CuInS_2$ QDs with different Cu^{2+} concentrations and (B) the fluorescence emission PL spectra of the as-prepared RNase A-$CuInS_2$ QDs at different reaction temperatures.

To further study the optical properties, the UV-vis spectra were also investigated in this study. Fig. 4 shows the UV–vis spectra of the RNase A-$CuInS_2$ QDs with the increasing Cu^{2+} concentration or the reaction temperature. As shown in Fig. 4A, there was a broad absorption peak in the long-wavelength region. As is known based on the previous research, the $CuInS_2$ QD nanocrystals typically did not show a well-defined exciton absorption due to their unique electronic properties. Specifically, a red-shift of the absorption band was observed, which might be caused by the growth of the QDs. Moreover, this abroad absorption peak of the QDs was observed in Fig. 4B, and it was red-shifted at a higher temperature, which was ascribed to the surface effects and the agglomeration of the QDs.

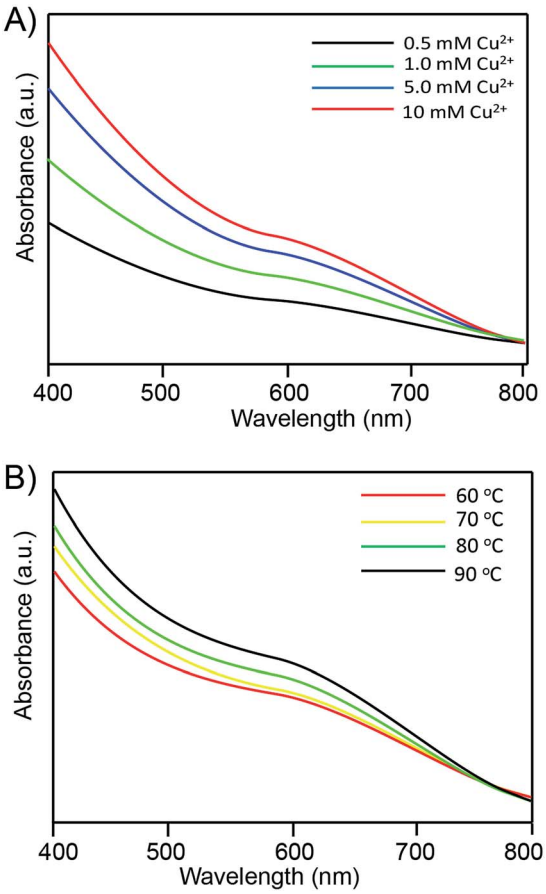

Fig. 4 The corresponding UV-vis absorption spectra of the RNase A-$CuInS_2$ QDs at (A) different Cu^{2+} precursor concentrations and (B) reaction temperatures.

The photoluminescence stability of the QDs

Compared with other organic dyes such as ICG, the QDs have been paid more attention due to their excellent optical properties such as the photostability. Therefore, the photostability of the RNase A-$CuInS_2$ QDs was further evaluated under different storage conditions such as buffer or temperature. Because biomolecules, such as protein, easily degraded or lost their activity, their fluorescence intensity could be affected. As shown in Fig. 5A, there were no obvious differences when our product was stored in either PBS buffer, distilled water or DMEM media at 24 h, 48 h, and 96 h. This result suggests that our as-prepared QDs have a good photostability in a biological environment that will be beneficial for their following biomedical applications. However, as shown in Fig. 5B, the fluorescence intensity of the RNase A-$CuInS_2$ QDs could dramatically decrease after 96 h storage at 60 °C, whereas their fluorescence intensity showed no changes at 4 °C and 37 °C. The decrease in fluorescence intensity could be ascribed to the self-assembly of the protein at high temperatures. Considering the physical condition of the human body (~37 °C), our product is very suitable for biomedical imaging because it has a good photostability in DMEM media at 37 °C in a short time. Notably, as shown in Fig. 5C, the as-prepared RNase A-$CuInS_2$ QDs exhibited a good photostability in a broad pH range from 2.3 to

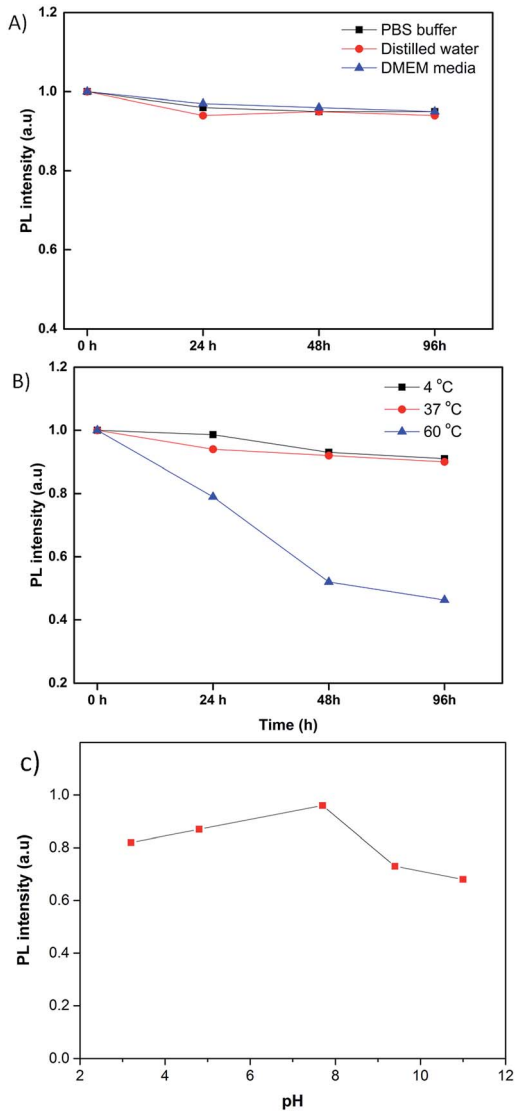

Fig. 5 The fluorescence intensity of the RNase A-CuInS$_2$ QDs stored in different buffers (A) and at different temperatures (B) and (C) pHs for 96 h.

11, at which the PL intensity remained more than 80% after the product was stored for 96 h. This phenomenon has also been observed in our previous studies,[21,26,27] which is mainly ascribed to the high stability of RNase A under both acidic and alkaline conditions. Particularly, the PL intensity of the QDs was higher under the acidic conditions than that under the alkaline conditions, whereas their maximum PL intensity was observed under the neutral condition (pH = 7). Considering that the pH in the stomach is around 3–5, our product can be used as an oral imaging agent for further applications in gastrointestinal system diseases.

The cytotoxicity of QDs

The biocompatibility of the RNase A-CuInS$_2$ QDs should be evaluated before further biomedical application. Fig. 6 displays the cell viability analysis of MC3T3-E1 cells treated with

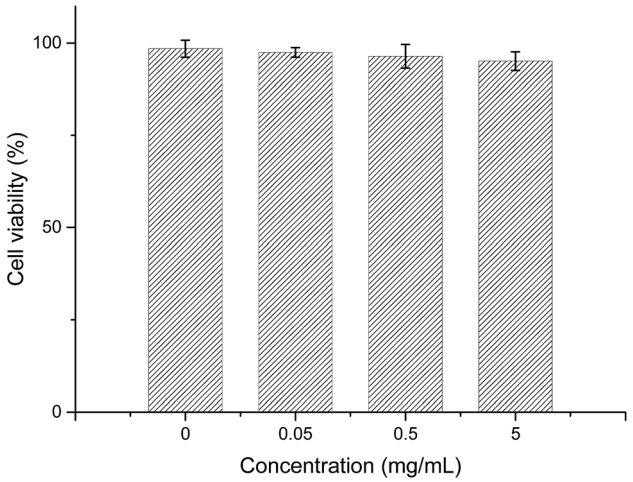

Fig. 6 Cell viability analysis of MC3T3-E1 cells incubated with different concentrations of the RNase A-CuInS$_2$ QDs after 24 h.

different concentrations of the RNase A-CuInS$_2$ QDs for 24 h. As shown in Fig. 6, the cell viability of MC3T3-E1 cells was still more than 95% even at a concentration of up to 5 mg mL^{-1} of the RNase A-CuInS$_2$ QDs. In this study, our QDs did not contain any toxic heavy ions such as Pb^{2+}, Cd^{2+}, or Hg^{+}, and the protein layer was around the surface of the QDs, which could make our product have a good biocompatibility.

In vivo imaging

To explore the *in vivo* imaging capability of the RNase A-CuInS$_2$ QDs, fluorescence imaging was performed in the mice after the injection. In this study, 200 μL of 50 mg mL^{-1} RNase A-CuInS$_2$ QDs in saline was injected into the tail of the mice. Fig. 7A and B show the fluorescence images of the mice before and after the injection, and it shows that the fluorescence signals of the QDs can be obviously observed after the injection. This result reveals that our prepared QDs are a good imaging agent for *in vivo* imaging. Particularly, as shown in Fig. 7B, there was only the fluorescence signal of the QDs without the fluorescence interference by the mice. This phenomenon is mainly ascribed to the low fluorescence background of the mice in the near-infrared region. Furthermore, the fluorescence signals of the QDs were still very clear after continuous excitation by a 808 nm laser for

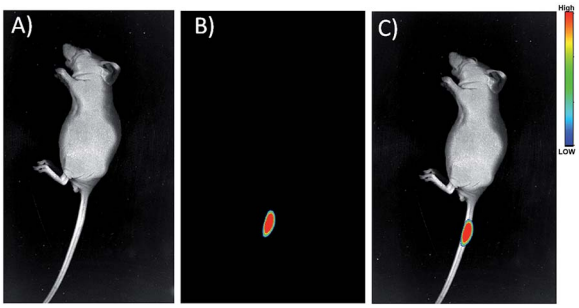

Fig. 7 (A) Bright light, (B) NIR fluorescence, and (C) merged images of the mice after treatment with the RNase A-CuInS$_2$ QDs.

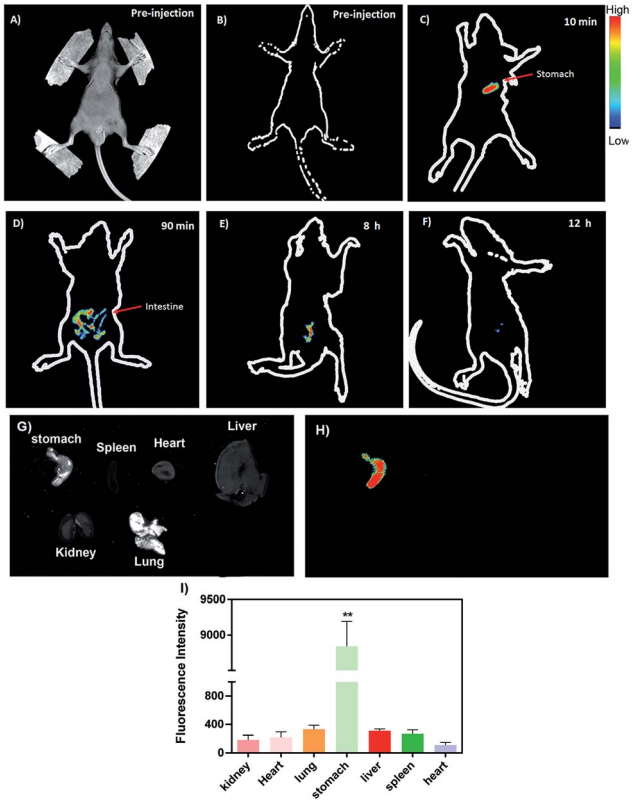

Fig. 8 (A) The bright light image and (B) the NIR fluorescence images of nude-mice before treatment. (C) to (F) *In vivo* NIR gastrointestinal tract imaging of the mice at various time intervals of the post-treatment. (G) and (H) The *ex vivo* imaging analysis of main organs of the mice after 10 min post-treatment. (I) The corresponding fluorescence intensity of the organs after 10 min post-treatment.

1 h and could be clearly observed after 24 h post-injection. Our product demonstrates better optical stability as compared to ICG. Very similar results were obtained by subcutaneous injecting into other places of the mice. Thus, the as-prepared RNase A-$CuInS_2$ QDs could be a better substitution of ICG for *in vivo* imaging in the future.

In vivo track imaging of QDs by oral administration

To further highlight its excellent optical properties for *in vivo* imaging, our product was delivered to the stomach of the mice using a gastric syringe, and the corresponding *in vivo* images were obtained at different time intervals. Fig. 8 illustrates the time-independent NIR images of the mice before and after the injection with our product. There was no obvious NIR signal before the injection, as shown in Fig. 8B. However, a bright NIR signal was observed in the stomach of the mice after oral administration of 200 μL of 50 mg mL^{-1} RNase A-$CuInS_2$ QDs, as shown in Fig. 8C, which clearly showed the outline of the stomach. Considering the depth and the acid condition of the stomach of nude-mice, the NIR image confirmed that the fluorescence signals of our product were strong and stable enough to be detected in the mice. Moreover, the signals could be mainly detected in the intestine of the mice after 90 min injection. Both the NIR area and the intensity of the QDs around

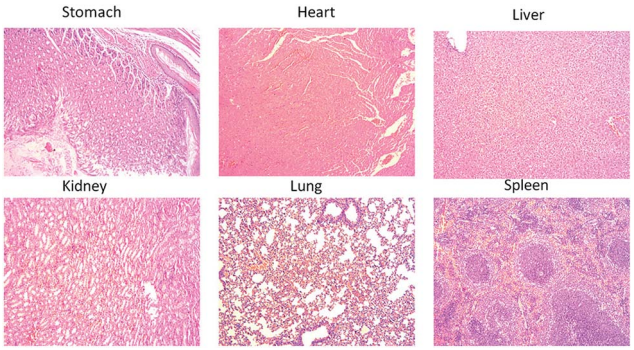

Fig. 9 (A) The corresponding hematoxylin-eosin (H&E) staining analysis of six organs (stomach, heart, liver, kidney, lung, and spleen) after 10 min post-treatment.

the intestine gradually decreased with the increasing time of post-injection. The *ex vivo* experiments showed that only in the stomach, significantly high NIR signals could be detected as compared to other organs of the mice (Fig. 8G to I); this which confirmed that the QDs were successfully delivered at the right position. Moreover, as shown in Fig. 9, the corresponding hematoxylin-eosin (H&E) staining analysis verified the previous cytotoxicity results indicating that there were no obvious toxic effects, such as immune response, caused by the QDs in the stomach as well as other important organs including heart, liver, lung, kidney, and spleen. These results of *ex vivo* analysis are consistent with the digestion *via* gastrointestinal system in the mice. In a word, these *in vivo* imaging results in both the tail tissue and the gastrointestinal system of the mice persuasively demonstrate the good *in vivo* imaging performance of the RNase A-$CuInS_2$ QDs with a deep tissue penetration and a good photostability.

Conclusions

In summary, we have demonstrated a one-pot synthesis of water-soluble NIR $CuInS_2$ QDs using RNase A as the template. Our product demonstrates an excellent NIR fluorescence intensity, a good stability, and a low cytotoxicity. The synthesis is green, straightforward, reproducible, and avoids the use of organic solvents such as TOPO. Particularly, the as-prepared RNase A-$CuInS_2$ QDs performed well in the following *in vivo* imaging experiment; this confirmed that they could be a good candidate for biomedical applications, especially in the gastrointestinal system.

Conflicts of interest

There are no conflicts to declare.

Acknowledgements

This project was supported by the National Natural Science Foundation of China (No. 81401771 and 81601879), the Natural Science Foundation of Shanghai Project (No. 15ZR1405000), the Innovation Program of the Shanghai Municipal Education Commission (No. 15ZZ006), the key clinical medicine center of

Shanghai (2017ZZ01006), the initial scientific research fund of Huashan Hospital (HSBY2016017) and the heath research projects of Health Department of Jiangsu Province (No. H2017071).

Notes and references

1 D. Murawa, K. Polom, Y. S. Rho and P. Murawa, *Contrast Media Mol. Imaging*, 2013, **8**, 211–219.
2 D. J. Burrington, *Laser Focus World*, 2015, **51**(11), 63.
3 F. Ris, R. Hompes, C. Cunningham, I. Lindsey, R. Guy, O. Jones, B. George, R. A. Cahill and N. J. Mortensen, *Surg. Endosc.*, 2014, **28**, 2221–2226.
4 Y. Junkichi, F. Mitsuhisa, O. Shinichi, A. Takashi, Y. Ryota, I. Shin, K. Masataka and I. Katsuhisa, *OncoTargets Ther.*, 2013, **6**, 325.
5 W. Hideyuki, H. Hoon, V. Christina, G. Julien, P. Gwangli, G. Sylvain, J. V. Frangioni, H. Maged and C. H. Soo, *Theranostics*, 2015, **5**, 1.
6 M. Fujimaki, J. Yokoyama, S. Ohba, T. Anzai, Y. Yoshii, S. Ito, M. Kojima and K. Ikeda, *Head Neck Oncol.*, 2012, **4**, 50.
7 S. Feng, J. Chen, W. Yan, Y. Li, S. Chen, Y. Zhang and W. Zhang, *Biomaterials*, 2016, **103**, 256–264.
8 I. A. Pestana, B. Coan, D. Erdmann, J. Marcus, L. S. Levin and M. R. Zenn, *Plast. Reconstr. Surg.*, 2009, **123**, 1239–1244.
9 M. I. Newman, M. C. Samson, J. F. Tamburrino, K. A. Swartz and L. Brunworth, *J. Reconstr. Microsurg.*, 2009, **19**, 1–5.
10 C. Holm, M. Mayr, E. Höfter, A. Becker, U. J. Pfeiffer and W. Mühlbauer, *Br. J. Plast. Surg.*, 2002, **55**, 635–644.
11 J. Chen, T. Zhang, L. Feng, M. Zhang, X. Zhang, H. Su and D. Cui, *Mater. Lett.*, 2013, **96**, 224–227.
12 J. O. Escobedo, O. Rusin, S. Lim and R. M. Strongin, *Curr. Opin. Chem. Biol.*, 2010, **14**, 64–70.
13 J. Yang, Y. Hu, J. Tan, L. Jia, Y.-H. Zhu and J.-S. Yu, *J. Mater. Chem. B*, 2015, **3**, 6928.
14 H. Chen, Y. Wang, J. Xu, J. Ji, J. Zhang, Y. Hu and Y. Gu, *J. Fluoresc.*, 2008, **18**, 801–811.
15 M. Yu, K. Zhao, X. Zhu, S. Tang, Z. Nie, Y. Huang, P. Zhao and S. Yao, *Biosens. Bioelectron.*, 2017, **95**, 41.
16 H. Chen, S. Cui, Z. Tu, J. Ji, J. Zhang and Y. Gu, *Photochem. Photobiol.*, 2011, **87**, 72–81.
17 J. Tao, P. Zhao and Q. Zeng, *J. Mater. Chem. B*, 2016, **4**, 4258–4262.
18 P. Zhao, K. He, Y. Han, Z. Zhang, M. Yu, H. Wang, Y. Huang, Z. Nie and S. Yao, *Anal. Chem.*, 2015, **87**, 9998.
19 T. Hu, W. Na, X. Yan and X. Su, *Talanta*, 2017, **165**, 194.
20 Y. Kong, J. Chen, F. Gao, W. Li, X. Xu, O. Pandoli, H. Yang, J. Ji and D. Cui, *Small*, 2010, **6**, 2367–2373.
21 J. Chen, Y. Kong, Y. Wo, H. Fang, Y. Li, T. Zhang, Y. Dong, Y. Ge, Z. Wu, D. Zhou and S. Chen, *J. Mater. Chem. B*, 2016, **4**, 6271–6278.
22 J. Chen, Y. Kong, W. Wang, H. Fang, Y. Wo, D. Zhou, Z. Wu, Y. Li and S. Chen, *Chem. Commun.*, 2016, **52**, 4025–4028.
23 J. Chen, Y. Kong, S. Feng, C. Chen, Y. Wo, W. Wang, Y. Dong, Z. Wu, Y. Li and S. Chen, *ACS Sustainable Chem. Eng.*, 2016, **4**, 2932–2938.
24 C. Jun, K. Yifei, J. Jiajia, R. Jing, W. Kan, G. Feng and C. Daxiang, *Nanoscale*, 2012, **4**, 4455–4458.
25 J. Chen, T. Zhang, L. Feng, X. Zhang, M. Zhang and D. Cui, *Micro Nano Lett.*, 2012, **7**, 1023–1025.
26 Y. F. Kong, J. Chen, F. Gao, R. Brydson, B. Johnson, G. Heath, Y. Zhang, L. Wu and D. J. Zhou, *Nanoscale*, 2013, **5**, 1009–1017.
27 Y. Kong, J. Chen, H. Fang, G. Heath, Y. Wo, W. Wang, Y. Li, Y. Guo, S. D. Evans, S. Chen and D. Zhou, *Chem. Mater.*, 2016, **28**, 3041–3050.

